JPE Journal of Photonics for Energy

RESEARCH PAPER

Techno-economic analysis of a solar thermophotovoltaic system for a residential building

Manish Mosalpuri,[a] **Fatima Toor**,[b,c] **and Mark Mba-Wright**[a,d,*]

[a]Iowa State University, Department of Mechanical Engineering, Ames, Iowa, United States
[b]University of Iowa, College of Engineering, Department of Electrical and Computer Engineering, Iowa City, Iowa, United States
[c]University of Iowa, College of Liberal Arts and Sciences, Department of Physics and Astronomy, Iowa City, Iowa, United States
[d]Iowa State University, Bioeconomy Institute, Ames, Iowa, United States

ABSTRACT. Thermophotovoltaics (TPV) is a technology that converts heat to electricity using a thermal emitter and a matched photovoltaic (PV) cell. TPV is becoming increasingly popular due to its advantages of silent power generation, higher power density (>2.5 W/cm^2), reduced cost, no moving parts (thus, low maintenance costs), reaching full power in less time as compared to turbines, operating at high temperatures, and suitability for long-duration energy storage applications. This study conducts a techno-economic analysis (TEA) of a solar energy conversion (using TPV) and storage system (using phase-change materials). We optimize the levelized cost of consumed energy (LCOE) and electricity ($LCOE_{el}$) using the Nelder-Mead algorithm for four scenarios (as identified in the reference study). These scenarios differ in nominal-weighted average cost of capital ($WACC_{nom}$), fuel and electricity inflation rate, and capital cost factor (CAPEX) of high-temperature energy storage (HTES), power generation unit (PGU), and PV systems. We perform a sensitivity analysis that predicts a modest decrease in LCOE and $LCOE_{el}$ from the mean values of \$0.038/kWh and \$0.128/kWh, respectively. We perform a Monte Carlo uncertainty assessment and fit a probability distribution based on input variables' historical data from the literature. The fitted probability distribution for outputs (mean, the standard deviation in brackets) is LCOE (\$/kWh)—general extreme value (0.035, 0.009), and $LCOE_{el}$ (\$/kWh)—*t* (0.132, 0.016). The reduced mean values for the optimized system indicate a massive potential for TPV to be economically feasible; however, the $LCOE_{el}$ is higher than the current average electricity price of \$0.124/kWh. The box plot shows that lifetime, PV CAPEX, inflation rate, natural gas price, and $WACC_{nom}$ significantly impact LCOE, and future research focused on them would lead to a better adoption of TPV technology.

 [DOI: 10.1117/1.JPE.14.042404]

Keywords: thermophotovoltaics; decarbonization; techno-economic analysis; Monte Carlo uncertainty assessment

Paper 24023SS received Apr. 26, 2024; revised Aug. 7, 2024; accepted Aug. 20, 2024; published Sep. 13, 2024.

1 Introduction

The adverse effects of climate change and global warming are showing up in numerous sectors, including agriculture, decrease in crop productivity;[1] food security, increase in food prices,[1]

*Address all correspondence to Mark Mba-Wright, markmw@iastate.edu

1947-7988/2024/$28.00

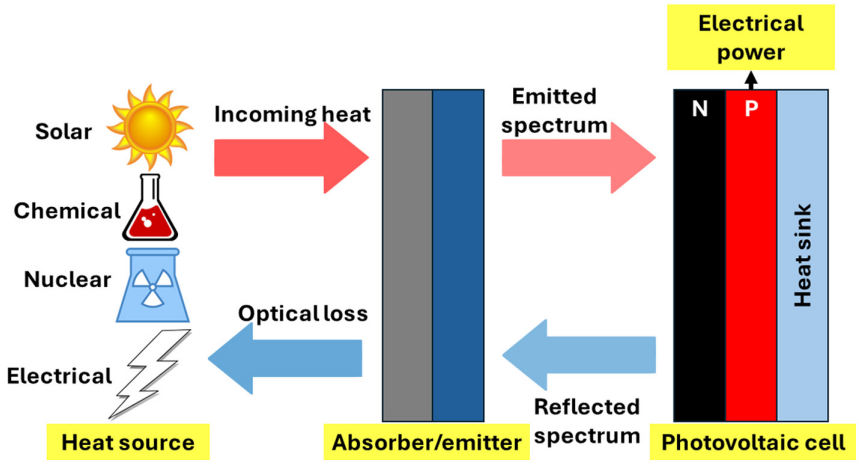

Fig. 1 TPV process schematic showing heat conversion to electrical power by the emitter and a PV cell (adapted from Burger et al.[12]).

food inequalities, and risks and uncertainty in local and global food systems;[2] biodiversity;[3–5] water resources;[6] and extreme weather events[7] and are set to worsen in the coming decades. To tackle these pressing impacts of climate change, a near-total decarbonization (carbon dioxide, CO_2 emission reduction by 50% to 90%) of the energy sector is recommended.[8] One of the best and the most prominent strategies to decarbonize the energy grid and limit global warming to 1.5°C (and thus reduce its harmful effects) is increasing the share of renewable energy technologies such as hydropower, solar photovoltaic (PV), and wind.[9,10] Some economists argue that supporting low-carbon technologies is the second-best strategy after carbon pricing.[11]

Thermophotovoltaics (TPV) is an emerging decarbonization and renewable energy technology that converts heat to electricity. Figure 1 shows the TPV process schematic. It requires a heat source that can be any of these four: solar, chemical, nuclear, or electrical.[13–15] The heat from these sources (in the range of 1300 to 2500 K)[13,16] or waste heat sources[17] are incident on the absorber/emitter, which converts it into radiation. The absorber/emitter acts as an infrared (IR) bandpass filter that absorbs IR photons from the heat source as a broadband blackbody spectrum and emits filtered IR photons matching the bandgap of the PV cell for efficient power conversion. An ideal emitter also serves as a heat barrier for the PV cell, blocking sub-bandgap photons emitted from the heat source. The overall TPV system efficiency (η_{TPV}) is defined in Eq. (1).[12,18]

$$\eta_{\mathrm{TPV}} = \frac{P_{\mathrm{out}}}{Q_h} = (\mathrm{SE.IQE})(\mathrm{VF})(\mathrm{FF})(\mathrm{CE}) = \left(J_{\mathrm{SC}} * \frac{V_g}{Q_{\mathrm{abs}}}\right) * \left(\frac{V_{\mathrm{OC}}}{V_G}\right) * \left[\frac{J_{\mathrm{mpp}} * V_{\mathrm{mpp}}}{J_{\mathrm{SC}} * V_{\mathrm{OC}}}\right] * \left(\frac{Q_{\mathrm{abs}}}{Q_h}\right), \tag{1}$$

where P_{out} is the generated electrical power, Q_h is the heat flow out of the emitter surface, SE is the spectral efficiency, IQE is the internal quantum efficiency (SE and IQE combined represent the amount of absorbed heat by the cell, Q_{abs} converting to the product of short-circuit current, J_{sc} and cell bandgap voltage, V_g), VF is the voltage factor (a measure of bandgap utilization, the ratio of open-circuit voltage, V_{OC} and bandgap voltage, V_g), FF is the fill factor (ratio of generated power, P_{out}, the product of maximum power point voltage, V_{mpp} and current, J_{mpp} and the product of J_{sc} and V_{OC}), and CE is the cavity efficiency (represents the emitter-cell combination effectiveness as a ratio of Q_{abs} and Q_h).[12]

1.1 Spectral Control

Spectral control refers to the employed techniques that increase the spectral efficiency by increasing the in-band radiation/photons that reach the PV cell. Spectral control in the TPV system is achieved using an IR emitter. There are two types of emitters: broadband and selective narrower band emitters. A broadband emitter emits a broad spectrum of blackbody radiation, which includes the undesired sub-bandgap photons. The sub-bandgap photons are reflected back into

the cell absorber using either a back-surface reflector (BSR) (silver (Ag), gold (Au), aluminum (Al),[19] etc.) or a front-surface filter (FSF) to enhance photon recycling in the PV cell, a common strategy to increase power efficiency of PV cells.[20] The sub-bandgap photons' reflection transfers the sub-bandgap light energy and prevents the PV cell from heating, which increases spectral efficiency and thus η_{TPV}[Eq. (1)]. Instead of using a BSR or an FSF, the emitter itself can be modified (called a selective emitter) using rare earth metals/oxides[21] to radiate only the valuable part of the spectrum. Selective emitter allows using a low-temperature emitter (400 to 1400 K), lower thermal stresses, a wide range of available materials, and improved material stability.[22,23] Selective emitters help reduce thermalization in PV cells but reduce the in-band power density.[24] The broadband emitters have higher in-band power density but reduce the overall efficiency; thus, both the broadband and selective emitters have tradeoffs, and a suitable emitter is chosen based on the application.

1.2 TPV Advantages

TPV is increasingly becoming popular as an energy conversion pathway due to its numerous applications, some of which include energy storage, combined heat and power[25] (CHP), waste energy recovery,[17,26] and in-space programs.[12,27] It can be used for CHP applications as it provides electricity and heat (it can also store heat due to its compatibility with storage applications). Due to its higher power density[12] (>2.5 W/cm^2) and reduced cost, there has been an increasing focus on energy storage using TPV, called thermal energy electrical storage (TEES) or thermal energy grid storage (TEGS) that is competitive with electrochemical batteries.[12,28] It also provides modular and silent power generation,[25] is compatible with a variety of fuels/heat sources (including waste heat), and has no moving parts (thus low maintenance costs). TPV is often compared with the most widespread method of power generation nowadays, power cycles using turbines. It reaches full power in less time as compared to turbines (starting time in order of seconds as compared with tens of minutes to an hour), operates at high temperatures[29] (due to its contact-less nature),[30] and is suitable for long-duration energy storage applications.[12,25] Due to material and technological constraints, turbines have an upper limit on the operating temperature, which is ~1500°C for the Brayton cycle and 700°C for the Rankine cycle. The efficiency upper limit is closely tied to this temperature limitation, around 38% for the Brayton cycle and 23% for the Rankine cycle.[27] TPV can operate at much higher temperatures (around 1700°C) and has an efficiency approaching 40%.[28] New TPV thermal energy storage technologies have the potential for commercialization and deployment at a large scale.[25] At the same time, turbine-based heat engines are high-risk applications due to their low efficiencies and thus require a significant capital investment.[29] The literature has several new studies related to the spectral control, prototyping, modeling, economic analysis, and energy storage applications of TPV systems.[31,32]

1.3 TPV Prototype and Modeling

There are a few models in the literature to predict experimental results from TPV technology and help it scale up and build a practical design for a prototype. Woolf et al.[33] modeled a TPV system consisting of a selective emitter, a dielectric filter, and a PV cell. They predicted accurate photovoltaic conversion efficiency with the model. Hassan et al.[34] modeled the optical (emitter-side spectral and spatial subsystem) and photovoltaic subsystems for a TPV system and observed the effects of emitter features on the optimum bandgap and overall efficiency. A recent innovative TPV study used machine learning to automatically model and optimize multilayer thin film structures to design an ideal spectral response.[35] Their deep learning-based model is efficient and accurate (to predict target spectra) and reduces resource consumption compared with complex numerical models.

1.4 TPV Economic Analyses

Some researchers have worked on evaluating the economic feasibility of TPV systems; however, it is still in its developing stages. Bianchi et al. (2012)[21,36] established an energy and economic evaluation framework for a TPV system for combined heat and power (CHP) application in a residential building. They calculate parameters such as primary and electrical energy consumption, primary energy savings, cost of electricity, and money savings. They conclude that the TPV system has immense potential as it reduces purchased grid electricity and increases monetary

savings. Fraas et al.[37] performed a preliminary techno-economic analysis (TEA) for a TPV furnace-generator system suitable for CHP applications. It consisted of a silicon carbide (SiC) radiant tube burner surrounded by a cylindrical silicon (Si)/gallium antimonide (GaSb) PV converter array, along with an antireflection-coated tungsten foil and an infrared filter over the cells to reduce out-of-band absorption. The system's electrical efficiency with a Si array and a standard furnace (without any furnace modifications) was found as 1.5% (and a power density of 0.3 Wcm^{-2}), and for a system with the low-bandgap GaSab cells, it was found as 15% (higher due to better spectral control, power density = 1 Wcm^{-2}). Their proposed TPV CHP unit would be economically feasible for integration into homes when the GaSb cells and arrays reach the desired low production cost. Their fuel-powered TPV system is suitable for distributed CHP applications and can be installed in homes for Winter, and renewable energy sources can be utilized in summer. Durisch and Bitnar propose a novel design of a self-powered residential electric heating system based on TPV technology.[38] Their system consists of a ytterbium oxide (Yb_2O_3) selective emitter and thin film solar cell materials (such as Si) or copper indium gallium selenide ($Cu(In,Ga)Se_2$) (CIGS). Thin film cells are typically 100 to 1000 times thinner than the conventional crystalline Si solar cells, thus saving extensive material and fabrication costs. Yb_2O_3 produces a selective emission spectrum and has a suitable bandgap to be used with Si or CIGS photocells. Their novel TPV system requires a production cost reduction to be feasible. However, it has the potential to be a basis for next-generation TPV technology to power off-grid homes and large-scale industries. The following section focuses on previous efforts in the literature on integrating energy storage and TPV and its economic feasibility.

1.5 Energy Storage Using TPV

Renewable energy sources such as solar PV and wind have the disadvantage of intermittency: they are only sometimes available throughout the day, which creates an imbalance between the load and energy generation (especially during peak hours). Energy storage technologies help tackle this problem by storing excess renewable energy that can be used when the energy required by the load is higher than the energy generated and thus would be an integral part of future grid networks to help increase power system flexibility and stability and ensure a smooth transition for decarbonization.[39,40] Electrochemical batteries (such as Li-ion) offer a cheap solution for energy storage due to the abundance of Li and other metals like cobalt and nickel used in electric vehicles and electricity storage batteries.[41] Low prices are due to excess supply and low demand, which did not meet the high demand expectations after the coronavirus disease (COVID-19) pandemic in 2020. Low demand might not encourage their mining in the future, but the demand is expected to go up; thus, there are high chances of high prices of these metals (and batteries). In this paper, we consider storing renewable and grid electricity as an emerging alternative to electrochemical batteries.

Storing electricity as heat, sometimes called electrothermal energy storage (ETES), is a possible solution to decarbonize industrial heating systems and can reduce up to 40% of 2022 global natural gas use and 14% of global energy greenhouse gas (GHG) emissions.[42] Many commercially available technologies for storing energy as sensible heat for industrial processes require high temperatures. Rondo Energy has designed a way to store excess renewable energy as high-temperature heat in insulated material at more than 1200°C for industrial applications.[43] Using renewable energy for industrial processes would help reduce its significant GHG emissions, especially from the two processes that release most emissions—the iron and steel industry[44] (ISI) and cement manufacturing.[45] The automotive and clean energy company Tesla mentions in its master plan for sustainable energy that thermal batteries (with an annual energy capacity of 41 TWh) can meet global electricity and transportation storage demand, along with renewables and other batteries.[46] Octopus energy uses artificial intelligence, machine learning, and its software system, Kraken, to balance power demand and supply using renewable energy storage technologies.[47] PV cell thermal energy storage technologies have the potential for commercialization and deployment at a large scale. In literature, there has been a focus on a few storage mediums, such as Si/Si alloys (phase-change materials, PCMs having high-energy densities $>$ 1 MWh/m^3 and low cost $< 4€/kWh = 4.31$ /kWh,[25,48] graphite,[49] Fe-Si-B alloy,[25,50] alumina fiber board.[51] For long-duration energy storage systems (10 to 100 h), it is essential to reduce the cost per unit energy (CPE) more than the cost per unit power (CPP) and round trip efficiency

(RTE).[25] Datas et al. analyzed a storage-integrated solar thermophotovoltaic (SISTPV) system, combining the TPV and PCMs.[52] They perform a steady-state analysis for a system using PCM to store incoming heat as latent heat, which is then used to produce electricity via the TPV system. Sensible heating systems need temperatures of more than 1500°C to operate, thus more challenging insulation requirements, but not latent heat units, as they operate at a constant discharge temperature. In a subsequent paper, they performed a transient analysis for the same SISTPV system.[53] They obtained promising results but mentioned that future technological improvements must be made to the model to perform an in-depth analysis. Datas et al.[30] designed a thermal energy storage system using phase change materials (PCMs) that convert electricity to latent heat (stored in PCM), which is then converted to electrical energy via TPV cells. Electricity is stored as heat in the PCM, which is inefficient, but it is economical to store heat that need not be converted to electricity due to heating loads.[25,49] As opposed to sensible heating storage mediums, latent heat provides the benefit of almost constant discharge temperature, which ensures the decoupling of energy storage and power generation capacity and operation at lower temperatures. They considered ideal TPV cells with 100% internal luminescent efficiency η_{int} (the fraction of electron-hole pairs that recombine radiatively within the semiconductor), a bandgap of 0.5 eV and BSR reflectivity of 80% and 100% (which denote the practical and ideal values, respectively). They obtained a maximum total energy density (thermal + electrical) of 1 MWh/m^3 and electrical energy densities of 200 to 600 kWh/m^3, comparable to the state-of-the-art lithium-ion (Li-ion) batteries. Datas et al.[25] estimate the levelized cost of electricity (LCOE), CPE, and CPP for a latent heat TPV (LHTPV) system. Their latent heat TPV (LHTPV) system stores the incoming power as heat with the help of a PCM (Si or FeSiB). First, the incoming power (from the grid or solar panels) is converted to heat via a heater (ohmic/induction/microwave/arc system) using an electric switch. The heat then melts the PCM (initially a solid), and the power is stored as latent heat in it. When the TPV cells are introduced into the system, the heat is transferred to the emitter of the TPV arrangement, and the PCM starts to solidify. For a detailed system embodiment, readers are referred to the original paper.[25] The PCM then converts heat to electricity as and when required with the help of a TPV cell. Amy et al.[29] presented a TEGS unit consisting of integrating energy storage with multi-junction PV (MPV) cells. In their proposed system, they first convert electricity to heat via joule heating of liquid Si. The heat is stored at 2400°C in a storage tank, then converted back to electricity on demand via MPV cells. They introduce a framework to evaluate economic feasibility using cost per unit energy (CPE), power (CPP), and the RTE.[29] They conclude that their TEGS system using MPV cells has the potential to be economically feasible and can enable high renewable energy penetration in the grid. Kelsall et al. modified the TEGS system presented by *Amy et al.* to include a multi-junction TPV cell, a solid graphite storage tank, and tin (Sn) as a heat-transfer fluid instead of liquid Si tanks.[19] This replacement by graphite and Sn is because of their advantages of low melting point and low solubility of Sn in graphite. Their TEA concludes that the CPE for their system can be below the target value of €20/kWh$_e$[54] (= 21.55/kWh$_e$) after the production capacity reaches a 100 MW target. A bottom-up TEA for highly concentrated PV modules suggests that the present PV cell cost can be reduced from a present value of €2/cm^2 to €0.2/cm^2 by reusing the substrate and reducing metallization costs, among other improvements.[55] Thus, there is an immense potential in energy storage using TPV, as seen from literature studies. Section 2 describes our methodology to obtain our economic analysis and uncertainty assessment results.

This study performs a techno-economic analysis and uncertainty assessment (using Monte Carlo simulations) and calculates the CO_2eq. emissions of energy storage using TPV. We are not aware of any literature studies performing Monte Carlo simulations for the TEA and CO_2eq. emissions of a TPV system. However, Monte Carlo simulations are essential for evaluating the uncertainty in input parameters, which is essential for evaluating the robustness of emerging TPV systems. The findings from this study could inform performance improvement targets and metrics for various grid resilience applications.

2 Methodology

We calculate and optimize the levelized cost of consumed energy (LCOE) and electricity (LCOE$_{\text{el}}$) for a TPV system for a typical residential building in Boone, Iowa, based on a model

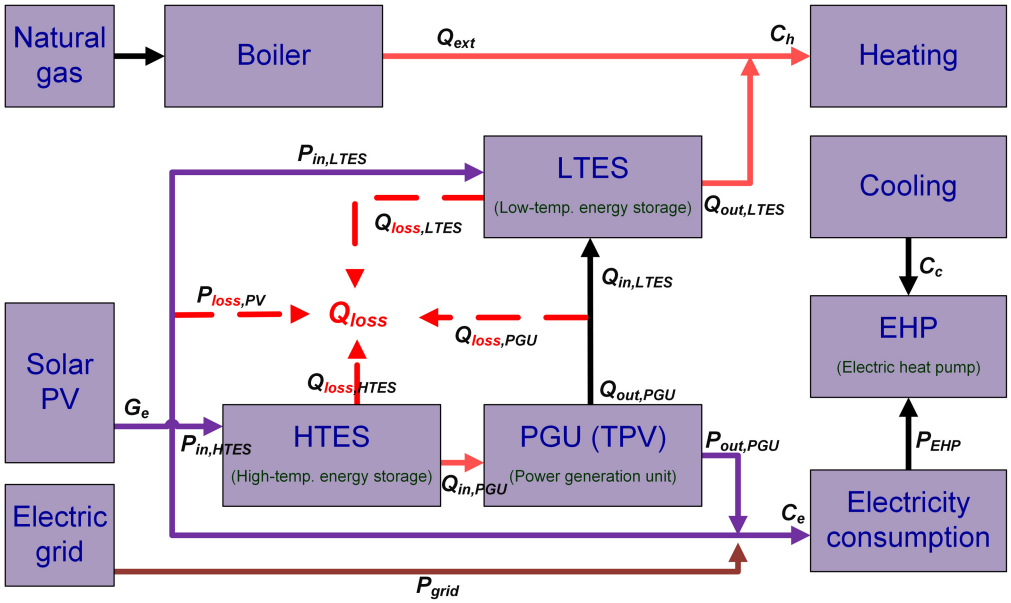

Fig. 2 System model showing energy sources and energy transfers to satisfy electricity consumption and heating and cooling loads (adapted from Datas et al.[56]).

built by Datas et al.[56] Their energy storage system is depicted in Fig. 2. It includes three energy sources—solar PV, electricity grid, and natural gas; a boiler (running on natural gas); two heat storages: low-temperature energy storage (LTES) and high-temperature energy storage (HTES); a power generation unit (PGU, here, it is a TPV unit); and a heat pump (either electric or thermal). Their energy management algorithm is shown in Fig. 10, along with our modifications highlighted in yellow. It computes the energy going into each storage based on the electric and heat demand and generation interplay. The algorithm details are provided in Appendix A.

We model this algorithm in Python (code available on GitHub[57] and explanation provided in Appendix E) and minimize LCOE and LCOE_{el}, using the Nelder-Mead algorithm by varying the power capacity of the PV (P_{nom}), HTES (HTES_{max}), and PGU (PGU_{max}) units. Nelder-Mead is a classic, direct search (no gradient knowledge needed) function minimization method that uses a simplex (function evaluations at different test points) and finds the following test points (the next simplex) using operations of reflection, expansion, contraction, and shrinkage.[58]

The inputs to the model are mentioned in Tables 1 and 2. LCOE and LCOE_{el} are defined in Eqs. (3) and (4). Minimizing LCOE_{el} also minimizes P_{grid} and increases the amount of electricity supplied from the HTES unit, as the LCOE_{el}'s operating expenditure (OPEX) term increases with P_{grid}, as observed in Eqs. (3) and (4).

To consider parameter uncertainty, we perform a scenario analysis (as performed in the reference study[56]) that calculates LCOE and LCOE_{el} based on current and future improvements and

Table 1 List of important input model parameters from the reference study[56] and a report by Lawrence Berkeley National Laboratory and the National Renewable Energy Laboratory.[59]

Input parameter	Value	Unit
HTES maximum capacity (optimized)	80	kWh_{th}
LTES maximum capacity (optimized)	80	kWh_{th}
PGU efficiency	25	%
PGU maximum generation capacity	1.5	kW_{el}
Building annual electricity consumption	7.73	MWh
Building annual heat consumption	39.63	MWh

Table 2 List of important input model economic parameters (capital cost of LTES unit, fixed cost of grid electricity, and fixed cost of fuel obtained from the reference study[56] and the rest from Monte Carlo distributions—see Fig. 3).

Input parameter	Value	Unit
Capital cost of PV unit	914.98	kW_{el}
Capital cost of PGU unit	1184.66	kW_{el}
Capital cost of HTES unit	118.4	kWh_{th}
Capital cost of LTES unit	32.32	kWh_{th}
Variable cost of grid electricity	0.124	kW_{el}
Fixed cost of grid electricity	53.87	kW_{el}/year
Variable cost of fuel	0.015	kWh_{th}
Fixed cost of fuel	64.65	kWh_{th}/year
Lifetime	24.34	years

Table 3 Scenario analysis inputs (prices converted to $ from €).

Scenario	$WACC_{nom}$ (%)	$Infl_{el}$ and $Infl_{fuel}$ (%)	$CAPEX_{HTES}$ ($/$kWh_{th}$)	$CAPEX_{PGU}$ ($/$kW_{el}$)	$CAPEX_{PV}$ ($/$kW_{el}$)
1 ($W_2I_4C_{32,323,970}$)	2	4	32.325	323.25	969.75
2 ($W_2I_4C_{108,970,1077}$)	2	4	107.75	1077.5	1293
3 ($W_3I_2C_{108,1077,1293}$)	3	2	107.75	1077.5	1293
4 ($W_3I_2C_{215,2155,1293}$)	3	2	215.5	2155	1293

tradeoffs in parameters such as HTES, PGU, PV capital cost, fuel ($Infl_{fuel}$), and electricity ($Infl_{el}$) inflation rates, and the nominal weighted average cost of capital ($WACC_{nom}$). It tells how the LCOE and $LCOE_{el}$ would change if the present parameters change in the future due to production scale-up and other changes. The scenarios are taken from the reference study and are mentioned in Table 3, where the original prices in € are converted to $.[60] From scenarios 1 to 4, the $WACC_{nom}$ and capital cost factor (CAPEX) values increase, and inflation rates decrease. The brackets in the first column mention an easier way of scenario representation. For example, scenario 1 is named $W_2I_4C_{32,323,970}$ as for this scenario, $WACC_{nom} = 2\%$, $Infl_{fuel} = Infl_{el} = 4\%$, and CAPEX of HTES ($CAPEX_{HTES}$), PGU ($CAPEX_{PGU}$), and PV ($CAPEX_{PV}$) = \$32/kWh_{th}, \$323/kW_{el}, and \$970/kW_{el}, respectively.

Sensitivity or scenario analysis does an excellent job of performing a preliminary uncertainty analysis by considering a range of values for the uncertain parameters. However, it does not adequately represent the uncertainty as they are still supplied as a fixed data point to the model at a time (there are still uncertainties within each parameter).[61,62] We thus perform a Monte Carlo uncertainty assessment to better model the uncertainty in some input parameters. The Monte Carlo method is an analysis tool that uses random numbers (generated using a probability distribution for each parameter) to calculate the output for a modeled stochastic process.[63]

The Monte Carlo method is already being used for advanced energy management algorithms for household systems,[64] renewable energy hubs,[65] and hospitals,[66] to name a few. It has also been used for TPV applications since 1997 when Gethers et al.[67] used it to track millions of photons from birth to death (by absorption or escape) and simulated individual probabilistic events sequentially to evaluate the TPV array's heat flux absorption and electrical performance. Since then, it has also been used to model TPV efficiency[68] and radiative energy transfer,[69] among other aspects.

The steps involved in the Monte Carlo method are listed in Appendix C.

Our modifications to the original LCOE and $LCOE_{el}$ minimization done in Datas et al.[56] are listed below:

a. Replacing the PGU unit with a TPV unit and using its actual efficiency values
b. Modifications to the original energy management algorithm, as shown in Fig. 10
c. Updating input parameter values obtained from the literature and using actual building energy consumption data
d. Providing a better estimate of LCOE and $LCOE_{el}$ after considering the uncertainty in input parameters via a Monte Carlo uncertainty analysis
e. Performing a sensitivity analysis and quantifying the total CO_2eq. emissions

3 Results and Discussion

First, we discuss the results obtained from the TEA of the TPV system for the scenarios in the reference study (scenario analysis results). We then conduct a TEA from the updated scenario inputs from the literature. We calculate the base case and optimized values for various parameters. The base-case value is the one without $LCOE/LCOE_{el}$ optimization and thus has a higher cost than the optimized case where the system size is varied for cost minimization.

3.1 Scenario Analysis Results

The results for scenario 1, $W_2I_4C_{32,323,970}$, are displayed in Table 4 based on the inputs listed in Tables 1, 2, and 3. We obtain the minimum base-case LCOE and $LCOE_{el}$ as \$0.046/kWh and \$0.17/kWh, respectively.

From Table 4, for the base-case scenario, the power obtained from the grid = 5.13 MW (= 55% of the total power demand), from solar PV = 3.93 MW (= 43% of the total power demand), and from the PGU (by stored energy in HTES) = 0.18 MWh (= 2% of the total power demand). These three sources satisfy entirely the power demand of 9.24 MW. HTES energy losses constitute 79% of the incoming solar PV energy into HTES (=3.59 MW), and the rest is mainly passed to the PGU (20%) or stored in HTES at the end of the year (less than 1%). These numbers change for the optimized case, represented in the fourth column of Table 4. HTES energy losses decrease to 66%, and the heat passed to the PGU increases to 33%. Less than 1% of

Table 4 Base-case and optimized inputs and results for scenario 1 ($W_2I_4C_{32,323,970}$).

Parameter	Base-case value	Optimized value	Unit
Solar PV size	9.5	5.0	kW
HTES maximum capacity	40.0	15.0	kWh_{th}
PGU maximum generation capacity	1.0	0.504	kW
Power obtained from the grid	5.13	4.99	MW
Power supplied from PGU/TPV by stored energy in HTES	0.18	0.31	MWh
Power supplied from PV	3.93	3.93	MW
Power supplied by the system	9.24		MW
Heat supplied from LTES	0.38	0.57	MWh
Heat supplied from the external boiler	39.25	39.06	MWh
Heat supplied by the system	39.63		MWh
Power generated from PV	7.73		MW
Total system losses	3.31	2.96	MWh
Self-consumption ratio	57.18	61.68	%
LCOE	0.046	0.041	\$/kWh

the energy is stored in HTES at the end of the year, as most of it is passed to the PGU to satisfy the electrical load. LTES supplies only 0.96% of the heating demand due to the algorithm's priority of HTES for energy storage over LTES (as defined in the reference study[56]). LTES stores energy only when it is not fully charged, and the HTES is either almost entirely (> 99%) or fully charged. The external boiler supplies the rest (99%) of the heating demand. These numbers improve modestly after optimizing LCOE, and the LTES supplies 1.5% of heating demand, and the external boiler supplies less energy = 98.5%. Thus, optimizing the system or searching for the least LCOE increases the energy supply from both the energy storages. Using the energy management algorithm is beneficial as it reduces the LCOE and increases solar PV's self-consumption ratio (SCR) from 57.2% to 61.7%. Less PV energy is lost, and the consumer utilizes more.

The SCR [defined in Eq. (2)] represents the amount of PV energy generated being utilized by the load either directly as electricity or indirectly as stored energy in HTES or LTES.

$$\text{Self} - \text{consumption ratio (SCR)} = 1 - \frac{\text{Total system losses}}{\text{Total PV power generated}}, \tag{2}$$

where total system losses = sum of energy losses from HTES, LTES, PGU, and PV systems.

The optimal system configuration is nominal PV capacity $(P_{\text{nom}}) = 5\ \text{kW}_{\text{el}}$, HTES maximum capacity $(\text{HTES}_{\text{max}}) = 15\ \text{kWh}_{\text{th}}$, and PGU maximum capacity $(\text{PGU}_{\text{max}}) = 0.504\ \text{kW}_{\text{el}}$. The base-case system configuration ($P_{\text{nom}} = 9.5\ \text{kW}_{\text{el}}$, $\text{HTES}_{\text{max}} = 40\ \text{kWh}_{\text{th}}$, and $\text{PGU}_{\text{max}} = 1.0\ \text{kW}$) converges to the minimum bounds for two optimized variables and is very close to the minimum for the third one, as seen in Table 5.

We observe that the optimal solution for the economically favorable scenarios (having lower WACC_{nom} and CAPEX values) converges to a somewhat larger PGU system, with its size being $0.504\ \text{kW}_{\text{el}}$ for scenario 1 ($W_2I_4C_{32,323,970}$). It obtains a lower P_{grid} (= 4.99 MWh), whereas small systems (nominal PV capacity = 5 kW_{el}, HTES max. capacity = 15 kWh_{th}, and PGU max. generation capacity = 0.5 kW_{el}) are obtained for unfavorable economic conditions, including high WACC_{nom} and high capital cost of HTES, PGU, and PV systems (their values mentioned in Table 5, column 1). Table 5 presents the scenario analysis results—the optimum system size (HTES, PGU, and nominal PV capacity) and the optimum LCOE and LCOE_{el} values. The base case and optimum LCOE and LCOE_{el} values are also shown in Fig. 3.

Unfavorable economic conditions produce a high optimum P_{grid} (=5 MWh for scenario 4:$W_3I_2C_{215,2155,1293}$). As economic conditions become favorable (low WACC_{nom} and low capital cost), we obtain a large PGU system, which becomes favorable to accommodate a large system (a large system is needed to store the produced PV energy). The same is true for LCOE_{el} minimization—scenario 1: $W_2I_4C_{32,323,970}$ (having the least WACC_{nom} and CAPEX) produces a system with PGU size = $0.519\ \text{kW}_{\text{el}}$. In comparison, all the rest scenarios converge on the lower bounds and give the result as nominal PV capacity = 5 kW_{el}, HTES max. capacity = 15 kWh_{th}, and PGU max. generation capacity = 0.5 kW_{el} (a small system). This phenomenon is illustrated in Appendix D, and an explanation is provided in Table 6.

The optimized LCOE and LCOE_{el} values mentioned in Table 5 seem counterintuitive: their values for the favorable scenario are higher than some unfavorable ones. This is due to the higher

Table 5 Scenario analysis results showing optimized system size (nominal PV capacity, HTES max. Capacity, and PGU max. generation capacity) and optimum LCOE and LCOE_{el} values.

	Optimized system size = [nominal PV capacity (kW_{el}), HTES max. capacity (kWh_{th}), PGU max. generation capacity (kW_{el})]		Optimum values	
Scenario	LCOE minimization	LCOE_{el} minimization	LCOE	LCOE_{el}
1 ($W_2I_4C_{32,323,970}$)	[5, 15, 0.504]	[5, 15, 0.519]	0.0403	0.144
2 ($W_2I_4C_{108,970,1077}$)	[5, 15,0.5]	[5, 15, 0.5]	0.0420	0.152
3 ($W_3I_2C_{108,1077,1293}$)	[5, 15, 0.5]	[5, 15, 0.5]	0.036	0.139
4 ($W_3I_2C_{215,2155,1293}$)	[5, 15, 0.5]	[5, 15, 0.5]	0.038	0.149

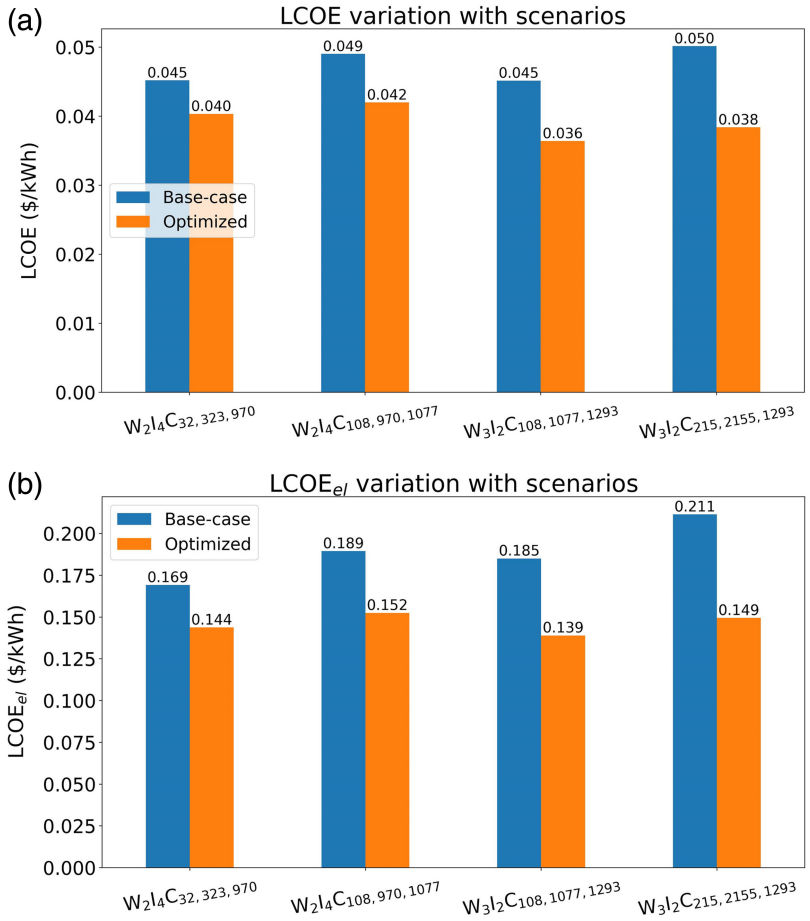

Fig. 3 Base-case and optimum (a) LCOE and (b) $LCOE_{el}$ variation with scenarios.

Table 6 Mean parameter values, as obtained from the Monte Carlo simulation fitted probability distributions.

Parameter	Mean value
Lifetime (years)	24.34
$WACC_{nom}$ (%)	2.17
PGU efficiency (%)	27.45
Electricity price ($/kWh)	0.124
$CAPEX_{PGU}$ ($/kW)	1184.66
$CAPEX_{PV}$ ($/kW)	914.98
$CAPEX_{HTES}$ ($/$kWh$_{th}$)	118.4
Inflation rate (%)	2.31
Natural gas price ($/kWh)	0.015

value of $Infl_{fuel}$ and $Infl_{el}$ for favorable cases, as assumed in the reference study. The LCOE equation [Eq. (3)] has two terms involving inflation rates, and $LCOE_{el}$ [Eq. (4)] just has one. This is why the effect is less pronounced for the $LCOE_{el}$ optimization case and more for LCOE. Scenario 3 ($W_3I_2C_{108,1077,1293}$) produces the least optimized LCOE and $LCOE_{el}$, as it has the right tradeoff between $WACC_{nom}$ and inflation rates.

3.2 Sensitivity Analysis and Monte Carlo Risk Assessment Results

Based on historical data from the literature, the fitted distribution for the non-triangular distributed parameters—natural gas price is a general extreme value, $Infl_{el}$ and $Infl_{fuel}$ is t; $CAPEX_{PV}$[70] is a general extreme value; and electricity price is Weibull distribution, as shown in Fig. 4, along with their 10 and 90% confidence interval limits.

Now, we mention the results from the scenario analysis we used for our study. First, the base-case and optimized LCOE and $LCOE_{el}$ for a mean scenario are illustrated in Fig. 5. For this scenario, we chose the mean parameter values (listed in Table 6 and Fig. 4) from the fitted Monte Carlo distributions. The values in Table 6 differ from the ones used in the four scenario analyses previously as those values were obtained from the reference study,[56] and these updated values are obtained from the fitted probability distributions.

LCOE and $LCOE_{el}$ are defined in Eqs. (3) and (4). LCOE represents the cost of supplying both heat and electricity; however, $LCOE_{el}$ only takes into account electricity costs. $LCOE_{el}$ was defined in the reference study as an alternative to LCOE to lower the payback period (LCOE minimization converges to a larger system, thus high investment and longer payback period) at the cost of obtaining a higher value for $LCOE_{el}$. For our study, Fig. 5 shows the base-case $LCOE_{el}$

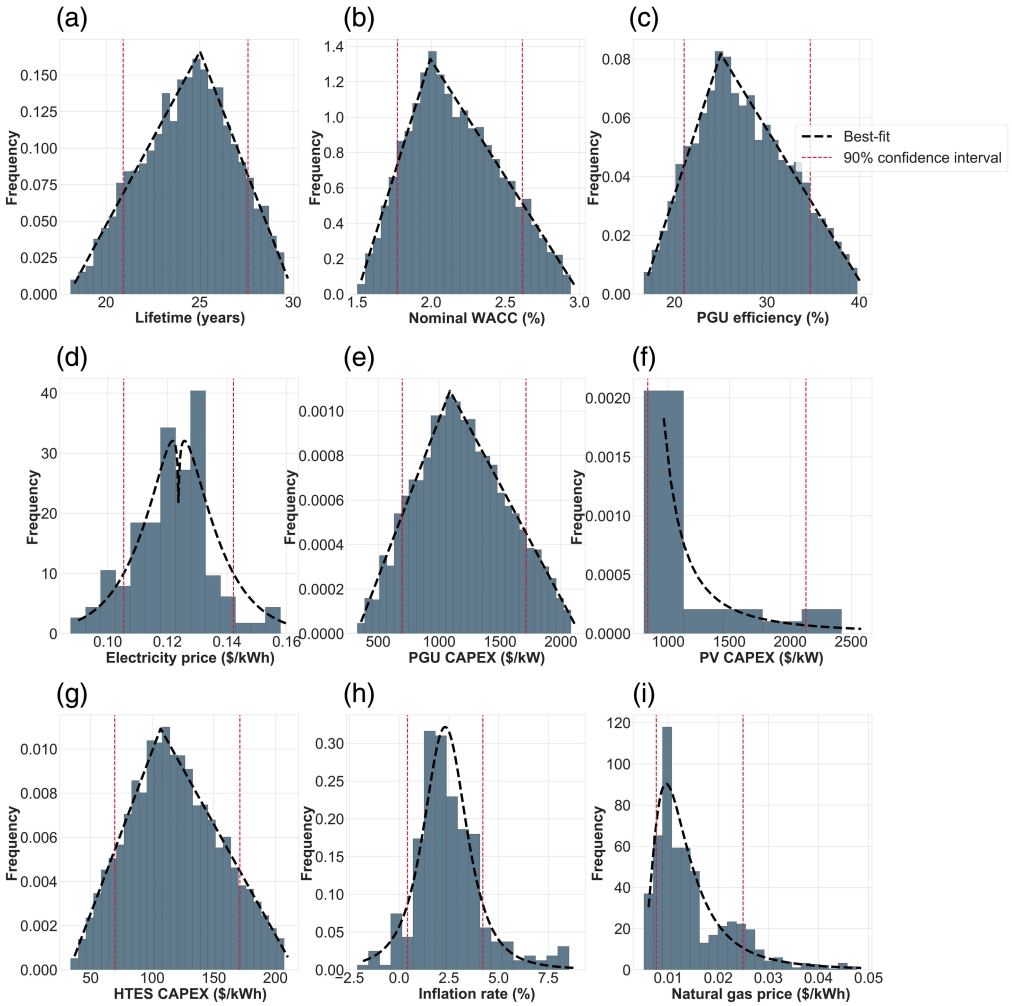

Fig. 4 Fitted probability distributions and 90% confidence limits for Monte Carlo parameters. Their distributions, mean, and standard deviation are as follows: (a) Lifetime (triangular distribution: 24.34 years, 2.47 years), (b) $WACC_{nom}$ (triangular distribution: 2.17%, 0.31%), (c) PGU efficiency (triangular distribution: 27.45%, 5.08%), (d) electricity price (Weibull distribution: \$0.124/kWh, \$0.015/kWh), (e) $CAPEX_{PGU}$ (triangular distribution: \$1184.66/kW, \$373.18/kW), (f) $CAPEX_{PV}$ (general extreme value distribution: \$914.98/kW, \$145.41/kW), (g) $CAPEX_{HTES}$ (triangular distribution: \$118.40/kWh, \$37.60/kWh), (h) inflation rates—$Infl_{fuel}$ and $Infl_{el}$ (t distribution: 2.31%, 2.11%), and (i) natural gas price (general extreme value distribution: \$0.015/kWh, \$0.011/kWh).

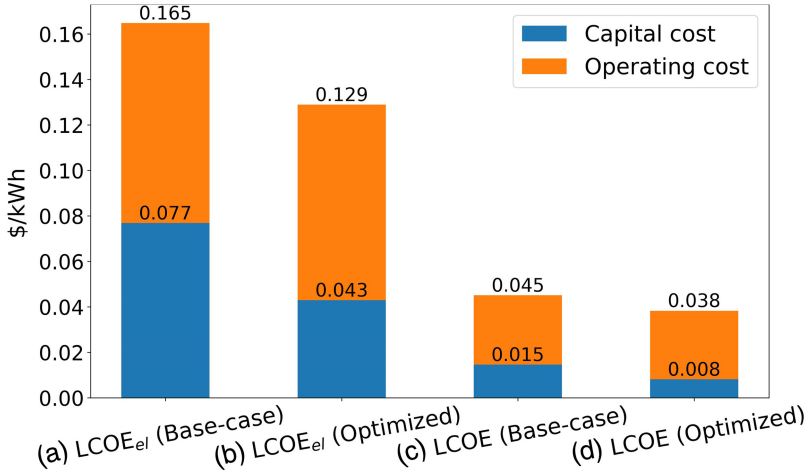

Fig. 5 Mean scenario (obtained from Monte Carlo results) analysis results for this study. The number on top of the bar denotes the total $LCOE_{el}$/LCOE, and the one below denotes the capital cost. (a) Base-case $LCOE_{el} = 0.165$/kWh. (b) Optimized $LCOE_{el} = 0.129$/kWh. (c) Base-case LCOE = \$0.045/kWh. (d) Optimized LCOE = \$0.038/kWh.

is \$0.165/kWh, which is reduced by 22% to \$0.129/kWh on optimization. The optimized value is very close to the average price of electricity obtained in Monte Carlo simulations (Fig. 4) = \$0.124/kWh. Energy storage using TPV can thus be profitable in the future. To assess future scenarios, we performed a sensitivity analysis and Monte Carlo simulations on the optimized system, which reduced LCOE and $LCOE_{el}$, and the results are mentioned in the next section.

LCOE has a much smaller value of \$0.045/kWh and optimizes to \$0.038/kWh. For both LCOE and $LCOE_{el}$, the optimum system converges to the smallest system size: nominal PV capacity = 5 kW_{el}, HTES max. capacity = 15 kWh_{th}, and PGU max. generation capacity $kW_{el} = 0.5$ kW. Based on this optimized system, we perform a sensitivity analysis based on the same parameters we considered for the uncertainty assessment. The results are displayed in Fig. 6 for parameters with values ±25% from the mean values listed in Table 6. The parameters having the most significant impact on LCOE and $LCOE_{el}$ are $Infl_{fuel}$ and $Infl_{el}$, electricity price, $CAPEX_{PV}$, lifetime, and natural gas price (only for LCOE), with a potential cost reduction of around 10% by the most dominant parameter (natural gas price for LCOE and $Infl_{fuel}$ and $Infl_{el}$ for $LCOE_{el}$). $LCOE_{el}$ does not change with natural gas prices because it only considers electricity, not heating requirements.

Figure 7 shows the Monte Carlo uncertainty assessment results for LCOE and $LCOE_{el}$ (for an optimized system: nominal PV capacity = 5 kW_{el}, HTES max. capacity = 15 kWh_{th}, PGU max. generation capacity $kW_{el} = 0.5$ kW). We depict the confidence intervals for our large sample analysis and do not rely on the *p*-values as they offer little insight for large samples.[71] The fitted distribution for LCOE is a general extreme value distribution, with a mean of \$0.035/kWh and a standard deviation of \$0.009/kWh, and that for $LCOE_{el}$ is a *t* distribution, with a mean of \$0.132/kWh and a standard deviation of \$0.016/kWh. The previously obtained optimized LCOE and $LCOE_{el}$ values listed in Table 5 (scenario analysis results) are within the 10% and 90% confidence limits. Thus, we obtained similar cost numbers to those in reference study[56] even after updating the assumptions and input values. The optimized LCOE from Fig. 6 is \$0.033/kWh, close to the mean (\$0.035/kWh) and median (\$0.039/kWh) values obtained here, and is much less than the electricity price mean (\$0.124/kWh), but is higher than the natural gas price mean (\$0.015/kWh). LCOE represents the cost of consumed energy (heat and electricity) and thus is compared with both mean values. Adding storage units and PV energy sources increases the price of the supplied energy, but it can be reduced, as shown in sensitivity analysis and uncertainty assessment results.

The optimized $LCOE_{el}$, as mentioned in Fig. 5, is \$0.129/kWh. The mean value calculated from the uncertainty analysis is close, \$0.132/kWh. Figure 7 depicts other statistical parameters such as standard deviation = \$0.016/kWh, 10%, and 90% confidence limits = (0.098, 0.165)

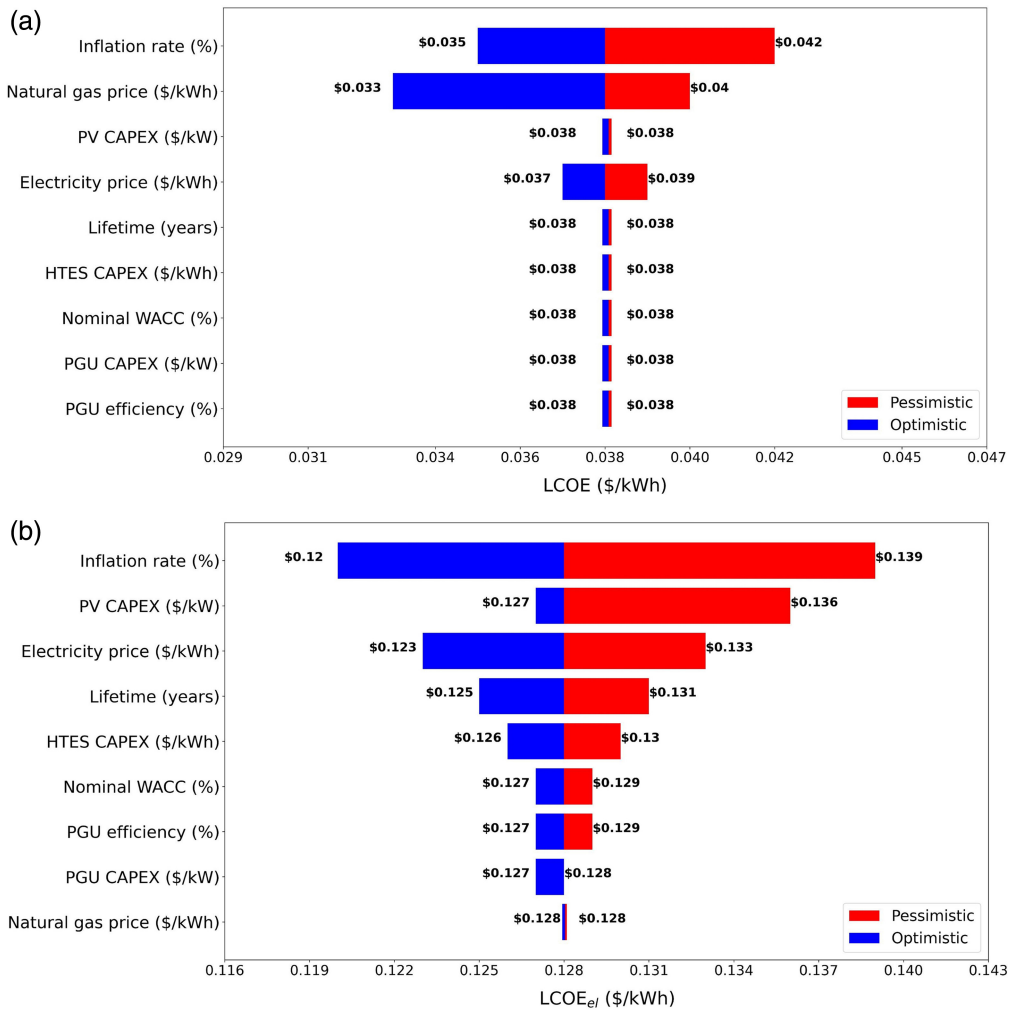

Fig. 6 Sensitivity analysis results for (a) LCOE and (b) $LCOE_{el}$ with parameter values ±25% from the mean values listed in Table 6.

$/kWh. It also shows the probability density function and the cumulative distribution function for LCOE and $LCOE_{el}$.

Box plots in Fig. 8 show the effects of each parameter's uncertainty on LCOE and $LCOE_{el}$. The boxes' left and right edges denote the 0.25 and 0.75 quartiles of the distributions (the width of the box is termed inter-quartile region, IQR), the dotted line inside the box indicates the median, and the whiskers and caps at the ends indicate the region from the box to the outermost data point within 1.5 times the IQR. Figure 8 illustrates that lifetime, $CAPEX_{PV}$, inflation rates, natural gas, and electricity prices have the most considerable impact on LCOE (the same parameters for sensitivity analysis). $LCOE_{el}$ has all the same dominant parameters (except natural gas price). A way to reduce LCOE and $LCOE_{el}$ would be to improve these parameters, as the boxes primarily lean towards the left (which implies lower cost). Thus, an improvement would lead to favorable economic results. The slightest uncertainty is observed in $CAPEX_{PGU}$ and PGU efficiency; in other words, their variation does not have much effect on LCOE and $LCOE_{el}$.

3.3 CO_2eq. Emission Results

Based on the results in Fig. 5, we calculate the CO_2eq. emissions from the energy system before and after optimization using emission factors listed in Table 7. Here, we use the emission factors for natural gas, grid electricity, and PV electricity and assume negligible emissions from the HTES, LTES, and PGU/TPV units due to a lack of literature data. The results are shown in Fig. 9. We observe that before using energy storage (using natural gas for heating and grid electricity), natural gas CO_2eq. emissions are the highest (=7.166 tons/year) and reduce modestly for

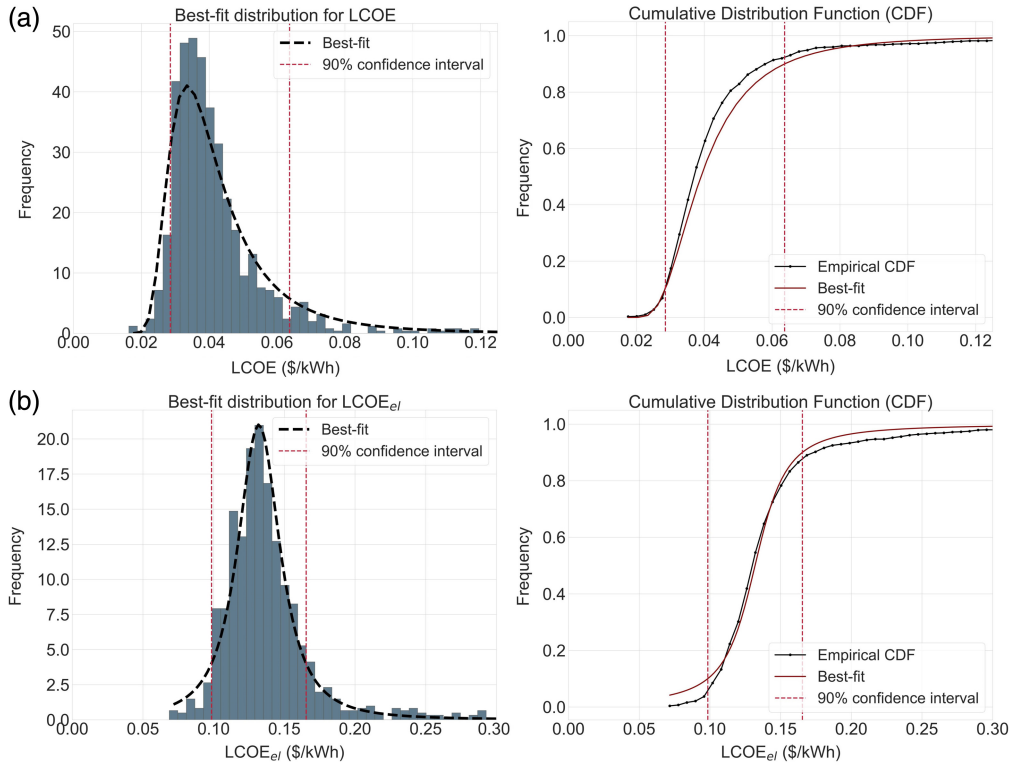

Fig. 7 Monte-Carlo risk uncertainty assessment results (probability density function, cumulative distribution function, 10% and 90% confidence limits) for (a) **LCOE**: mean = 0.035, median = 0.039, standard deviation = 0.009, 10% and 90% confidence limits = (0.028,0.064) (all in $/kWh) and (b) **LCOE$_{el}$**: mean = 0.132, median = 0.132, standard deviation = 0.016, 10% and 90% confidence limits = (0.098, 0.165) (all in $/kWh).

the base case and optimized cases (both use energy storage). The total CO_2eq. emissions for the system with no energy storage are 9.98 tons/year. The total emissions reduce for the base case (*b*) = 8.824 tons/year due to lesser dependence on natural gas and grid electricity and more utilization of cleaner solar PV energy to supply heat and electricity. The emissions are the lowest for the optimized case (*c*) (=8.75 tons/year) due to an optimized system with less dependence on grid electricity and an external boiler. Thus, according to our results, utilizing the energy management algorithm for energy storage and optimizing the system reduces CO_2eq. emissions by a modest amount (12%), primarily due to less dependence on grid electricity. Renewable energy integration in future grids would reduce their environmental impact; thus, TPV energy storage inclusion might not significantly reduce emissions. However, a detailed life cycle assessment must be performed to understand the process emissions better.

4 Conclusions and Future Work

Decarbonization using renewable energy is vital to achieving the environmental targets set by the IPCC to keep global warming below 1.5°C. This paper performs a techno-economic analysis and uncertainty assessment for a renewable energy technology, thermophotovoltaics (TPV). TPV research is still in the beginning stages, with no working large-scale prototypes. Our analysis shows that TPV still needs to be economically feasible based on previous scenarios from the literature and updated inputs from the results of Monte Carlo simulations, but it has immense potential. According to the authors' knowledge, this is the first study that performs an uncertainty assessment of the TPV technology. The critical results, conclusions, and future work from the study are listed below:

1. From the scenario analysis (based on reference study data), we obtain a minimum LCOE of $0.036/kWh and a minimum LCOE$_{el}$ of $0.139/kWh. These values are for the scenario

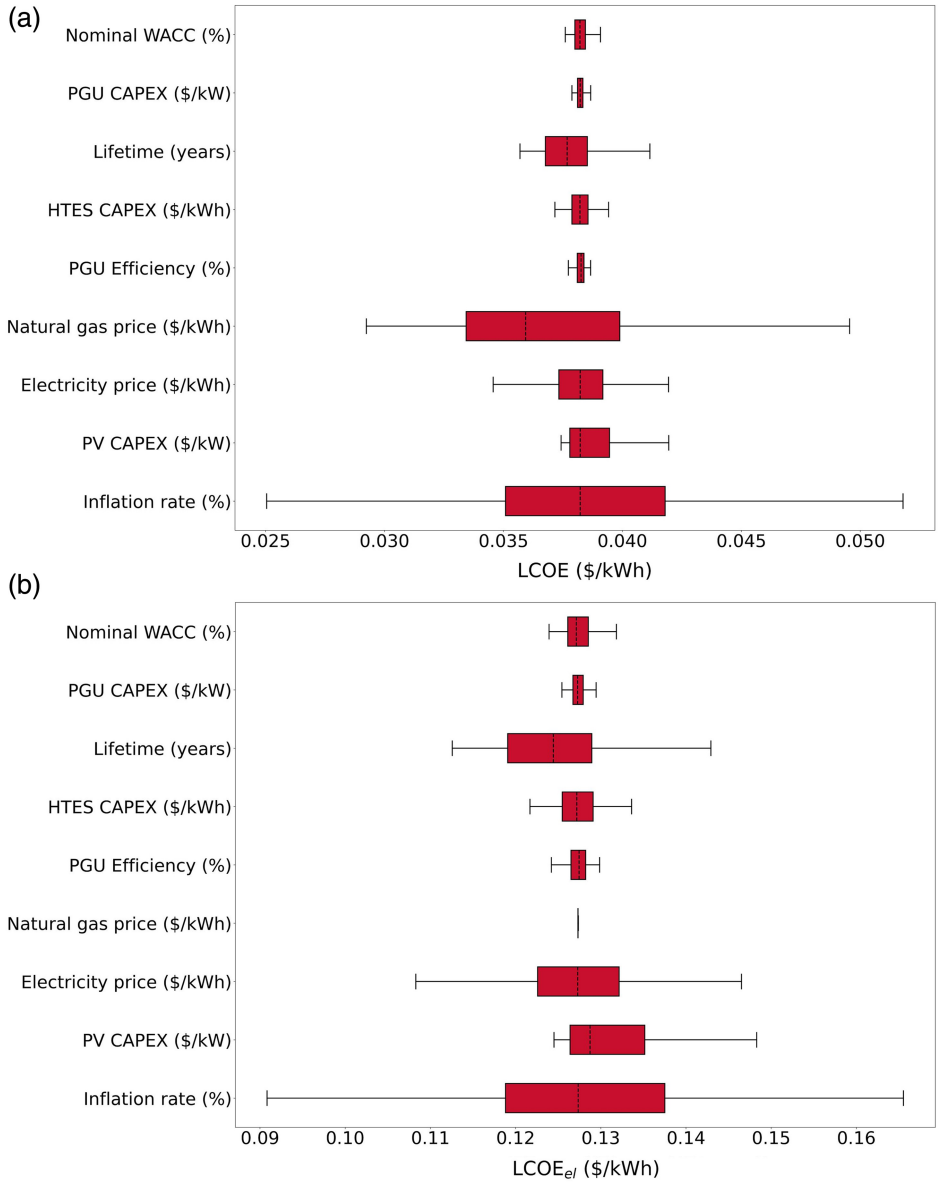

Fig. 8 (a) LCOE and (b) $LCOE_{el}$ box plot representing parameter uncertainty.

Table 7 Emission factors for natural gas, grid electricity, and PV electricity.

Parameter	Value
Natural gas emission factor (gCO_2eq/kWh_{th})	180.78[72]
Grid electricity emission factor (gCO_2eq/kWh_{el})	304.14[73]
PV electricity emission factor (gCO_2eq/kWh_{el})	43.00[74]

$W_3I_2C_{108,1077,1293}$, where $WACC_{nom} = 3\%$, $Infl_{fuel} = Infl_{el} = 2\%$, $CAPEX_{HTES} = 108/kWh_{th}$, $CAPEX_{PGU} = 1077/kW_{el}$, and $CAPEX_{PV} = 1293/kW_{el}$.

2. For the mean scenario (obtained from Monte Carlo results), base-case $LCOE_{el} = 0.165/kWh$, optimized $LCOE_{el} = 0.129/kWh$; base-case LCOE = \$0.045/kWh, and optimized LCOE = \$0.038/kWh. For both LCOE and $LCOE_{el}$, the optimum system

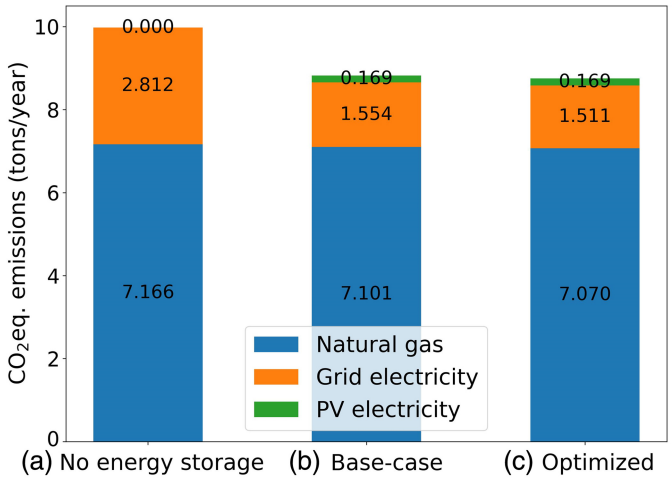

Fig. 9 CO_2eq. emissions in tons/year for (a) without energy storage (heat and electricity obtained from an external boiler and the grid, respectively), (b) base case, and (c) optimized case. For each column, the numbers represent the emissions from natural gas, grid electricity, and solar PV electricity (going from bottom to top).

converges to the smallest system size: nominal PV capacity = 5 kW_{el}, HTES max. capacity = 15 kWh_{th}, PGU max. generation capacity $kW_{el} = 0.5$ kW.

3. The sensitivity analysis results show that the parameters having the most significant impact on LCOE and $LCOE_{el}$ are inflation rates ($Infl_{fuel}$ and $Infl_{el}$), electricity price, $CAPEX_{PV}$, lifetime, and natural gas price (only for LCOE), with a potential cost reduction of around 10% by the most dominant parameter (natural gas price for LCOE and $Infl_{fuel}$ and $Infl_{el}$ for $LCOE_{el}$).
4. According to the Monte Carlo simulations, the fitted distribution for LCOE is a general extreme value distribution, with a mean of \$0.035/kWh and a standard deviation of \$0.009/kWh, and that for $LCOE_{el}$ is a t distribution, with a mean of \$0.132/kWh and a standard deviation of \$0.016/kWh.
5. Box plot results show that the lifetime, $CAPEX_{PV}$, inflation rates, natural gas price, and electricity price significantly impact LCOE (the same parameters for sensitivity analysis). $LCOE_{el}$ has all the same dominant parameters (except natural gas price). A way to reduce LCOE and $LCOE_{el}$ would be to improve these parameters; thus, there is an immense potential for economic feasibility for TPV in the future.
6. According to the CO_2eq. emissions results, the total CO_2eq. emissions for the system with no energy storage are 9.98 tons/year, for the base case are 8.824 tons/year, and for the optimized case are 8.75 tons/year. Utilizing the energy management algorithm for energy storage and optimizing the system reduces CO_2eq. emissions by a modest amount (12%) due to lesser dependence on natural gas for heating and grid electricity and higher utilization of renewable solar PV energy.

5 Appendix A: Energy Management Algorithm

The energy management algorithm is shown in Fig. 10, along with our modifications highlighted in yellow. It computes the energy going into each storage based on the electric and heat demand and generation interplay.

The algorithm by Datas et al.[56] follows this approach (which requires an input of power consumed by the load and that produced by the solar PV system per hour): first, it computes if there is excess electricity produced by the solar PV system $[P_g(t)]$ compared with the electricity consumption $[P_c(t)]$. If yes, the excess energy is stored in HTES (which stores heat at high temperature to supply to the PGU unit) if it is not fully charged; if it is fully charged and there is a heating load, it is stored in LTES (which stores heat at low temperature and supplies it for space and domestic hot water heating); if even this is full, this energy is lost.

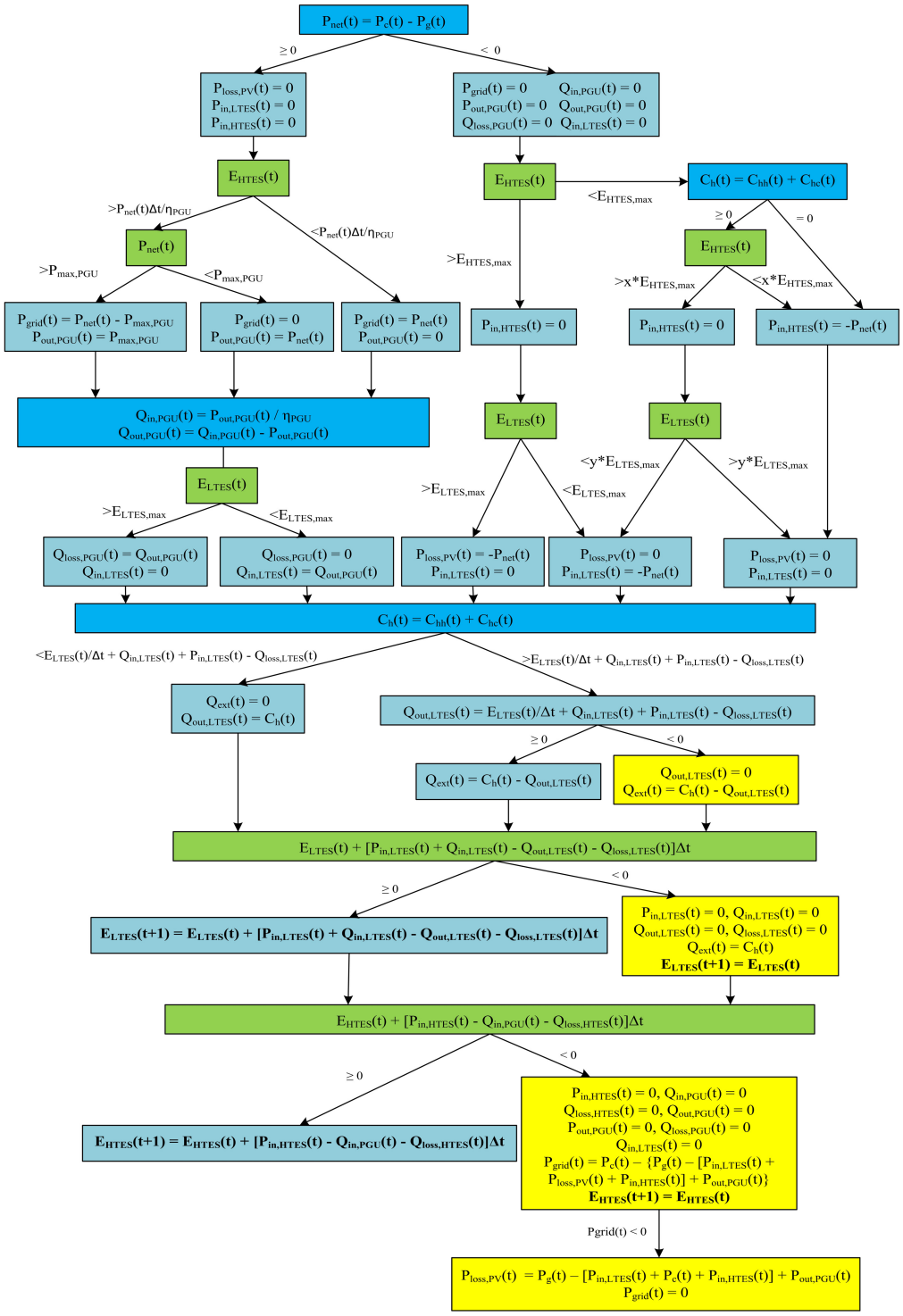

Fig. 10 Energy management algorithm from the reference study,[56] with our modifications highlighted in yellow.

We modify their algorithm as the energy storage terms (E_{HTES} and E_{LTES}) for the $(t+1)$th interval turn negative when their respective loss terms ($Q_{\mathrm{loss,HTES}}$ and $Q_{\mathrm{loss,LTES}}$) begin to dominate in the mass balance equation. In this modification, we make these assumptions:

1. When the loss term starts to dominate, it is possible to cut off the respective energy storage unit. When $Q_{\mathrm{loss,LTES}}$ dominates, we shut off the LTES unit for that iteration (all the inputs and outputs are turned down to zero), the stored energy, E_{LTES} (t), is carried forward to the

$(t+1)$th interval, and the heat loads are supplied energy from the external boiler. Similarly, for the HTES unit, when $Q_{loss,HTES}$ dominates, we shut it off for that iteration (all the inputs and outputs are turned down to zero). The stored energy, $E_{HTES}(t)$, is carried forward to the $(t+1)$th interval, and the required electricity for that interval is supplied from the grid $(=P_{grid})$. There were a few instances when P_{grid} turned out negative because electricity generation was more significant than consumption. Solar PV supplies all the electricity in that case, and P_{grid} is reduced to 0.

2. When the heat output from LTES ($Q_{out,LTES}$) is calculated as negative (due to the large value of $E_{loss,LTES}$), it is possible to obtain the required heat energy from the external boiler and not use LTES for that iteration.

The modifications we made are for the building energy values we considered, thus might not work very well for other buildings. We suggest that researchers first use the original code from the reference study and then decide whether our modifications are required for their building. A benefit of using the modifications is that we would not obtain negative values for stored energy if the loss terms dominate. However, a limitation is that cutting off the storage units or connecting them back to the system in real time might be challenging.

6 Appendix B: LCOE, $LCOE_{el}$, and Operating Expenditure (OPEX) Equations

LCOE and $LCOE_{el}$ are defined in Eqs. (3) and (4).

$$\mathrm{LCOE} = \frac{\mathrm{CAPEX} + \sum_{t=1}^{T}\left[\frac{\mathrm{OPEX}(t)}{(1+\mathrm{WACC_{nom}})^t}\right]}{\sum_{t=1}^{T}\left[\frac{\sum_{t=1}^{8760}(c_e(t)+c_h(t))\Delta t}{(1+\mathrm{WACC_{real}})^t}\right]}, \tag{3}$$

where

$$\mathrm{OPEX}(t) = (1+\mathrm{Infl_{el}})^t\left\{\mathrm{OPEX^*_{elec,fix}}\max[P_{grid}(t) + \mathrm{OPEX^*_{elec,var}}\sum_{t=1}^{8760}P_{grid}(t)\Delta t\right\}$$
$$+ (1+\mathrm{Infl_{fuel}})^t\left\{\mathrm{OPEX^*_{fuel,fix}} + \mathrm{OPEX^*_{fuel,var}}\sum_{t=1}^{8760}Q_{ext}(t)\Delta t\right\}$$

$$\mathrm{LCOE_{el}} = \frac{\mathrm{CAPEX} + \sum_{t=1}^{T}\left[\frac{\mathrm{OPEX_{el}}(t)}{(1+\mathrm{WACC_{nom}})^t}\right]}{\sum_{t=1}^{T}\left[\frac{\sum_{t=1}^{8760}c_e(t)\Delta t}{(1+\mathrm{WACC_{real}})^t}\right]}, \tag{4}$$

where

$$\mathrm{OPEX_{el}}(t) = (1+\mathrm{Infl_{el}})^t\left\{\mathrm{OPEX^*_{elec,fix}}\max[P_{grid}(t) + \mathrm{OPEX^*_{elec,var}}\sum_{t=1}^{8760}P_{grid}(t)\Delta t\right\}$$

where CAPEX is equal to the total capital expenditure of the system, $C_e(t)$ is the electricity consumption, $C_h(t)$ is heat consumption, $\mathrm{WACC_{real}}$ is the real weighted average cost of capital, $\mathrm{OPEX*_{elec,fix}}$, $\mathrm{OPEX*_{elec,var}}$, $\mathrm{OPEX*_{fuel,fix}}$, and $\mathrm{OPEX*_{fuel,var}}$ represent the fixed and variable cost factors for fuel and electricity, and $Q_{ext}(t)$ is the heat obtained from the external boiler.

7 Appendix C: Monte Carlo Uncertainty Assessment Methodology

The steps involved in the Monte Carlo method are listed below:

1. The first step is identifying the key parameters to participate in the method. We use the same parameters as we did for the scenario analysis. We also consider these additional parameters—natural gas price, electricity price, PGU/TPV efficiency, and project lifetime.
2. The second step is identifying a best-fit probability distribution for each parameter. We fit a triangular distribution for $\mathrm{WACC_{nom}}$, $\mathrm{CAPEX_{HTES}}$, $\mathrm{CAPEX_{PGU}}$, PGU efficiency, and

lifetime. We specify their lowest, most probable (mode), and highest values to generate a triangular distribution, which attempts to cover the range of values. For other parameters (natural gas price, Infl_{el}, and $\text{Infl}_{\text{fuel}}$, CAPEX_{PV}, and electricity price), we obtain their historical data from the literature, and the distfit python package v1.4.0 identifies and fits their probability distributions (shown in Fig. 6 of the main text).[75] Here, we assume the historical parameters' variation would guide future variation in the form of probability distributions.

3. The next step is to generate random numbers (5000 for our study) from the specified distributions for all the parameters and supply them, one at a time, to the Python algorithm model, which generates an empirical distribution for the output variables (LCOE and LCOE_{el}). A data frame stores the LCOE and LCOE_{el} values for each parameter input from the random data set. Here, we choose the number of samples as 5000 as the results (mean and standard deviation) converged for numbers greater than it (tolerance limit = 10^{-3}). We ran each simulation ten times.
4. The last step is to analyze the mean, standard deviation, significance, and uncertainty levels of LCOE and LCOE_{el}.

8 Appendix D: Scenario Analysis Results

Figure 11 shows that the smallest bounds have the lowest LCOE for scenario 4: $W_3I_2C_{215,2155,1293}$, whereas for scenario 1, $W_2I_4C_{32,323,970}$, the optimum is not always at the smallest system size. The PGU maximum capacity has an optimum LCOE at around 1 kW_{el}—favorable economic conditions can accommodate a larger system with lower cost. This is the reason we obtain larger systems for favorable economic conditions. The variation of LCOE with PGU max. generation capacity for scenario 1 shows a discontinuous variation for the most part. It is due to the direct effect of PGU capacity on P_{grid} (see the code), which affects the operating expenditure—an exponent function (summed over the entire lifetime of the project) to calculate LCOE (the non-linear variation of operating expenditure dominates the linear variation of capital expenditure). PGU capacity thus updates P_{grid} and the power output from PGU at each time

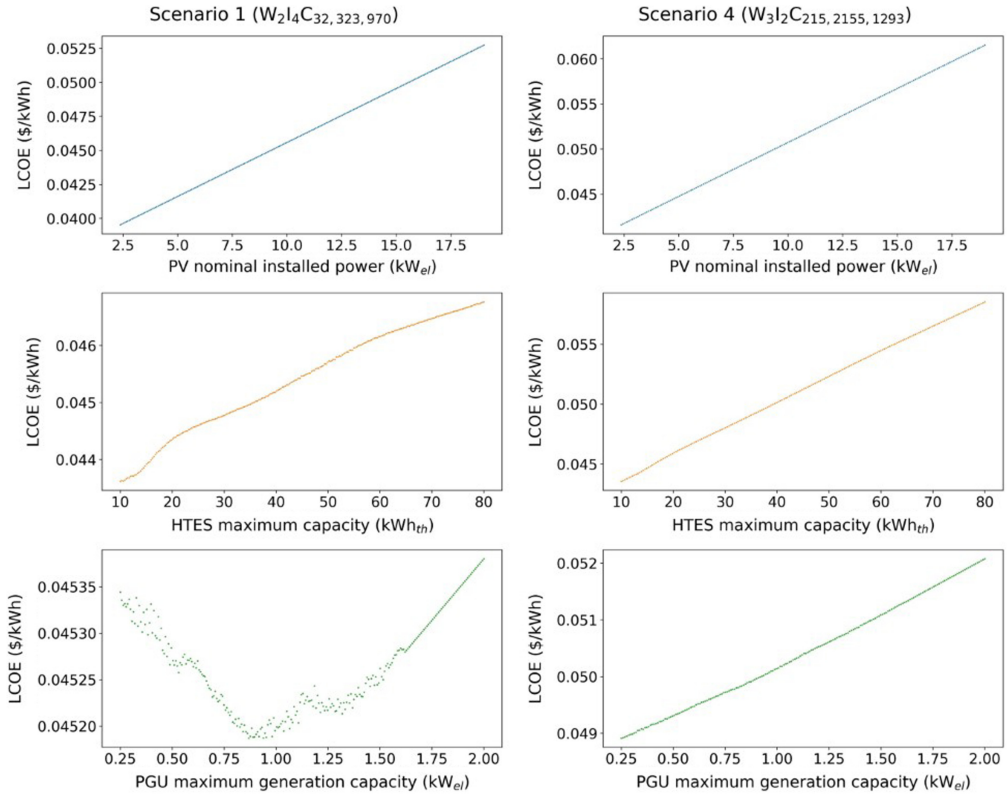

Fig. 11 LCOE ($/kWh) variation with economic scenarios and system size.

interval (and is responsible for LCOE fluctuations), which is not valid for the other two variables plotted in Fig. 5 (main text)—PV and HTES capacities are not directly involved in the calculation of the operating expenditure (an exponent function); they have a linear relationship with capital expenditure, and thus, they have a continuous variation. Scenario 1 variation of LCOE with PGU capacity is discontinuous. In contrast, scenario 4 is smooth and continuous as it has higher capital expenditure (and low-operating expenditure), which dominates LCOE and produces a linear variation.

9 Appendix E: GitHub Code

Our code allows anyone with their own input parameters to calculate the optimized LCOE and $LCOE_{el}$ for their building's energy storage system. Readers who wish to use our code as a template are encouraged to go through the comments in the code for a better understanding.

In the GitHub link,[57] follow these instructions:

1. The file "Optimization_and_CO2_emissions.py" contains the code to calculate and optimize the levelized cost of energy (LCOE) and electricity ($LCOE_{el}$) by following the energy management algorithm from the original study (ref: https://doi.org/10.1016/j.apenergy.2019.113935) along with our modifications according to our needs. It imports the Excel file "TPV.xlsx" that contains the hourly electricity consumption and solar PV generation data for a residential building in Boone, Iowa. The Python file also plots the base case and optimized LCOE and $LCOE_{el}$. It also calculates the CO_2eq. emissions for a building with no energy storage system and base case and optimized energy storage systems with a TPV unit.
2. The file "Monte_Carlo_uncertainty_analysis.py" performs the Monte Carlo uncertainty assessment on some input parameters by importing their historical data from the literature (from the Excel file "Monte_Carlo_parameters.xlsx"). It then fits a probability distribution to each parameter and supplies their values to the model to calculate LCOE. Then, it plots the probability distribution and cumulative distribution functions for LCOE (for an optimized system).

Disclosures

We have no relevant financial interests in the paper and no other potential conflicts of interest to disclose.

Code and Data Availability

The data presented in this article are publicly available in the ThermoPhotoVoltaics repository at https://zenodo.org/doi/10.5281/zenodo.10988244

Acknowledgments

The authors gratefully acknowledge the funding for the work by the Decarb 2040 Community Feasibility Grant Program.

References

1. A. Calzadilla et al., "Climate change impacts on global agriculture," *Clim. Change* **120**(1–2), 357–374 (2013).
2. T. Wheeler, "Climate change impacts on global food security," *Science* **341**, 508–513 (2013).
3. S. C. Doney et al., "Climate change impacts on marine ecosystems," *Annu. Rev. Mar. Sci.* **4**(1), 11–37 (2012).
4. C. Bellard et al., "Impacts of climate change on the future of biodiversity," *Ecol. Lett.* **15**(4), 365–377 (2012).
5. J. Gross, "Coral reefs are in trouble. One lab in the desert is trying to help," *The New York Times*, 13 December 2023, https://www.nytimes.com/2023/12/13/climate/emirates-coral-restoration.html?searchResultPosition=10 (accessed 19 December 2023).
6. B. Sivakumar, "Global climate change and its impacts on water resources planning and management: assessment and challenges," *Stoch. Environ. Res. Risk Assess.* **25**(4), 583–600 (2011).

7. D. Erdenesanaa, "A year of 'unreal' fire and warming in the arctic," *The New York Times*, 12 December 2023, https://www.nytimes.com/2023/12/12/climate/arctic-report-card-climate-change.html?searchResultPosition=18 (accessed 19 December 2023).
8. P. J. Loftus et al., "A critical review of global decarbonization scenarios: what do they tell us about feasibility?," *WIREs Clim. Change* **6**(1), 93–112 (2015).
9. Intergovernmental Panel on Climate Change, *Global warming of 1.5°C. An IPCC special report on the impacts of global warming of 1.5°C above pre-industrial levels and related global greenhouse gas emission pathways, in the context of strengthening the global response to the threat of climate change, sustainable development, and efforts to eradicate poverty*, IPCC, https://www.ipcc.ch/sr15/ (2018); Vol. 616, Cambridge University Press (2022).
10. E. Papadis and G. Tsatsaronis, "Challenges in the decarbonization of the energy sector," *Energy* **205**, 118025 (2020).
11. J. Meckling, T. Sterner, and G. Wagner, "Policy sequencing toward decarbonization," *Nat. Energy* **2**(12), 918–922 (2017).
12. T. Burger et al., "Present efficiencies and future opportunities in thermophotovoltaics," *Joule* **4**(8), 1660–1680 (2020).
13. Z. Zhou et al., "Solar thermophotovoltaics: reshaping the solar spectrum," *Nanophotonics* **5**(1), 1–21 (2016).
14. B. Wernsman, "Advanced thermophotovoltaic devices for space nuclear power systems," *AIP Conf. Proc.* **746**, 1441–1448 (2005).
15. K. Qiu and A. C. S. Hayden, "Implementation of a TPV integrated boiler for micro-CHP in residential buildings," *Appl. Energy* **134**, 143–149 (2014).
16. H. Daneshvar, R. Prinja, and N. P. Kherani, "Thermophotovoltaics: fundamentals, challenges and prospects," *Appl. Energy* **159**, 560–575 (2015).
17. A. Licht et al., "A review of advances in thermophotovoltaics for power generation and waste heat harvesting," *MRS Adv.* **4**(41–42), 2271–2282 (2019).
18. R. Sakakibara et al., "Practical emitters for thermophotovoltaics: a review," *J. Photonics Energy* **9**(3), 032713 (2019).
19. J. Fernández et al., "Back-surface optimization of germanium TPV cells," *AIP Conf. Proc.* **890**, 190–197 (2007).
20. T. Bauer, *Thermophotovoltaics: Basic Principles and Critical Aspects of System Design* (Chapter 3), Green Energy and Technology, Springer Berlin Heidelberg, Berlin, Heidelberg (2011).
21. J. M. Baker and T. J. Griffis, "Feasibility of recycling excess agricultural nitrate with electrodialysis," *J. Environ. Qual.* **46**(6), 1528–1534 (2017).
22. W. R. Chan et al., "Toward high-energy-density, high-efficiency, and moderate-temperature chip-scale thermophotovoltaics," *Proc. Natl. Acad. Sci. U. S. A.* **110**(14), 5309–5314 (2013).
23. D. Fan et al., "Near-perfect photon utilization in an air-bridge thermophotovoltaic cell," *Nature* **586**(7828), 237–241 (2020).
24. S. Molesky, C. J. Dewalt, and Z. Jacob, "High temperature epsilon-near-zero and epsilon-near-pole metamaterial emitters for thermophotovoltaics," *Opt. Express* **21**(S1), A96 (2013).
25. A. Datas et al., "Latent heat thermophotovoltaic batteries," *Joule* **6**(2), 418–443 (2022).
26. K. Park et al., "Performance analysis of near-field thermophotovoltaic devices considering absorption distribution," *J. Quantum Spectrosc. Radiat. Transf.* **109**(2), 305–316 (2008).
27. A. Datas and A. Martí, "Thermophotovoltaic energy in space applications: review and future potential," *Sol. Energy Mater. Sol. Cells* **161**, 285–296 (2017).
28. A. LaPotin et al., "Thermophotovoltaic efficiency of 40%," *Nature* **604**(7905), 287–291 (2022).
29. C. Amy et al., "Thermal energy grid storage using multi-junction photovoltaics," *Energy Environ. Sci.* **12**(1), 334–343 (2019).
30. A. Datas et al., "Ultra high temperature latent heat energy storage and thermophotovoltaic energy conversion," *Energy* **107**, 542–549 (2016).
31. M. M. A. Gamel et al., "A review on thermophotovoltaic cell and its applications in energy conversion: issues and recommendations," *Materials* **14**(17), 4944 (2021).
32. K. F. Mustafa et al., "A review of combustion-driven thermoelectric (TE) and thermophotovoltaic (TPV) power systems," *Renew. Sustain. Energy Rev.* **71**, 572–584 (2017).
33. D. N. Woolf et al., "High-efficiency thermophotovoltaic energy conversion enabled by a metamaterial selective emitter," *Optica* **5**(2), 213 (2018).
34. S. Hassan, C. F. Doiron, and G. V. Naik, "Optimum selective emitters for efficient thermophotovoltaic conversion," *Appl. Phys. Lett.* **116**(2) (2020).
35. Q. Pan et al., "Deep learning-based inverse design optimization of efficient multilayer thermal emitters in the near-infrared broad spectrum," *Opt. Express* **31**(15), 23944 (2023).
36. M. Bianchi et al., "Feasibility study of a thermo-photo-voltaic system for CHP application in residential buildings," *Appl. Energy* **97**, 704–713 (2012).

37. L. M. Fraas, J. E. Avery, and H. X. Huang, "Thermophotovoltaic furnace-generator for the home using low bandgap GaSb cells," *Semicond. Sci. Technol.* **18**(5), S247 (2003).
38. W. Durisch and B. Bitnar, "Novel thin film thermophotovoltaic system," *Sol. Energy Mater. Sol. Cells* **94**(6), 960–965 (2010).
39. A. Castillo and D. F. Gayme, "Grid-scale energy storage applications in renewable energy integration: a survey," *Energy Convers. Manag.* **87**, 885–894 (2014).
40. M. Jafari, A. Botterud, and A. Sakti, "Decarbonizing power systems: a critical review of the role of energy storage," *Renew. Sustain. Energy Rev.* **158**, 112077 (2022).
41. Y. Khan, "Low battery metal prices set to persist in 2024, adding friction to energy transition," The Wall Street Journal. December 28, 2023, https://www.wsj.com/articles/low-battery-metal-prices-set-to-persist-in-2024-adding-friction-to-energy-transition-3773ba00?&mod=djemSustainableBusinessPro (accessed 1 April 2024).
42. M. Guan et al., "Catalysing the global opportunity for electrothermal energy storage," 2024, https://www.systemiq.earth/wp-content/uploads/2024/03/Global-ETES-Opportunity-Report-240227.pdf (accessed 21 March 2024).
43. E. Ballard, "Startup wants to store spare renewable electricity to power heavy industry," The Wall Street Journal, February 8, 2022, https://www.wsj.com/articles/startup-wants-to-store-spare-renewable-electricity-to-power-heavy-industry-11644328800?mod=djemclimate (accessed 21 October 2023).
44. R. Wu, Z. Tan, and B. Lin, "Does carbon emission trading scheme really improve the CO_2 emission efficiency? Evidence from China's Iron and Steel Industry," *Energy* **277**, 127743 (2023).
45. R. Kajaste and M. Hurme, "Cement industry greenhouse gas emissions–management options and abatement cost," *J. Clean. Prod.* **112**, 4041–4052 (2016).
46. "Master plan Part 3- sustainable energy for all of Earth," TESLA, 2023, https://www.tesla.com/ns_videos/Tesla-Master-Plan-Part-3.pdf (accessed 21 December 2023).
47. R. Toplensky, "Octopus energy has Texas-size ambitions," The Wall Street Journal, January 4, 2024, https://www.wsj.com/articles/octopus-energy-has-texas-size-ambitions-6f11cfb8?mod=djemSustainableBusinessPro (accessed 4 January 2024).
48. C. Amy et al., "High-temperature pumping of silicon for thermal energy grid storage," *Energy* **233**, 121105 (2021).
49. C. C. Kelsall, K. Buznitsky, and A. Henry, "Technoeconomic analysis of thermal energy grid storage using graphite and tin," 2021, http://arxiv.org/abs/2106.07624 (accessed 25 July 2023).
50. J. Jiao et al., "The use of eutectic Fe-Si-B alloy as a phase change material in thermal energy storage systems," *Materials* **12**(14), 2312 (2019).
51. S. Lang, H. Drück, and D. Bestenlehner, Chap. 8 in "Ultrahigh temperature thermal insulation," in *Ultra-high temperature thermal energy storage, transfer and conversion*, pp. 201–219, Elsevier (2021).
52. A. Datas, D. L. Chubb, and A. Veeraragavan, "Steady state analysis of a storage integrated solar thermophotovoltaic (SISTPV) system," *Sol. Energy* **96**, 33–45 (2013).
53. A. Veeraragavan, L. Montgomery, and A. Datas, "Night time performance of a storage integrated solar thermophotovoltaic (SISTPV) system," *Sol. Energy* **108**, 377–389 (2014).
54. P. Albertus, J. S. Manser, and S. Litzelman, "Long-duration electricity storage applications, economics, and technologies," *Joule* **4**(1), 21–32 (2020).
55. K. A. W. Horowitz et al., "A bottom-up cost analysis of a high concentration PV module," *AIP Conf. Proc.* **1679**, 100001 (1679).
56. A. Datas, A. Ramos, and C. del Cañizo, "Techno-economic analysis of solar PV power-to-heat-to-power storage and trigeneration in the residential sector," *Appl. Energy* **256**, 113935 (2019).
57. M. Mosalpuri, "Python code for techno-economic analysis and uncertainty assessment of thermophotovoltaics technology," GitHub, https://github.com/manishm211/ThermoPhotoVoltaics (accessed 16 April 2024).
58. J. A. Nelder and R. Mead, "A simplex method for function minimization," *Comput. J.* **7**(4), 308–313 (1965).
59. N. M. Frick et al., "End-use load profiles for the U.S. building stock: market needs, use cases, and data gaps," DE-AC0205CH11231, 2019. https://www.nrel.gov/docs/fy20osti/75215.pdf (accessed 10 April 2024).
60. Google Finance, "Euro to United States dollar," https://www.google.com/finance/quote/EUR-USD?sa=X&ved=2ahUKEwjr-5i7opyEAxXhj4kEHTtdCtQQmY0JegQIBxAv (accessed 8 February 2024).
61. S. Greenland, "Sensitivity analysis, Monte Carlo risk analysis, and Bayesian uncertainty assessment," *Risk Anal.* **21**(4), 579–584 (2001).
62. B. Li et al., "Techno-economic and uncertainty analysis of in situ and ex situ fast pyrolysis for biofuel production," *Bioresour. Technol.* **196**, 49–56 (2015).
63. M. H. Kalos and P. A. Whitlock, Chap. 1 in "What is Monte Carlo?," in *Monte Carlo Methods*, pp. 1–5, Wiley-VCH Verlag GmbH & Co. KGaA (2008).
64. S. Arens et al., "Monte-Carlo evaluation of residential energy system morphologies applying device agnostic energy management," *IEEE Access* **10**, 7460–7475 (2022).

65. A. Tavakoli and A. Karimi, "Development of Monte-Carlo-based stochastic scenarios to improve uncertainty modelling for optimal energy management of a renewable energy hub," *IET Renew. Power Gener.* **17**(5), 1139–1164 (2023).
66. G. Mavrotas, K. Florios, and D. Vlachou, "Energy planning of a hospital using mathematical programming and Monte Carlo simulation for dealing with uncertainty in the economic parameters," *Energy Convers. Manage.* **51**(4), 722–731 (2010).
67. C. K. Gethers et al., "TPV efficiency predictions and measurements for a closed cavity geometry," in *Third NREL Conf. thermophotovolt. Gener. of Electr.*, ASCE, Colorado Springs, Colorado, pp. 471–486 (1997).
68. R. Liu et al., "Simulation of edge effects in thermophotovoltaic efficiency by Monte Carlo calculation," *AIP Adv.* **13**(2), 025263 (2023).
69. J. Aschaber, C. Hebling, and J. Luther, "Realistic modelling of TPV systems," *Semicond. Sci. Technol.* **18**(5), S158–S164 (2003).
70. National Renewable Energy Laboratory (NREL), "Residential PV annual technology baseline," Annual Technology Baseline, https://atb.nrel.gov/electricity/2022/residential_pv (accessed 1 June 2024).
71. M. Lin, H. C. Lucas, and G. Shmueli, "Too big to fail: large samples and the p-value problem," *Inf. Syst. Res.* **24**(4), 906–917 (2013).
72. United States Environmental Protection Agency (EPA), "Greenhouse gases equivalencies calculator–calculations and references," Energy and the Environment, https://www.epa.gov/energy/greenhouse-gases-equivalencies-calculator-calculations-and-references#:~:text=The%20average%20carbon%20dioxide%20coefficient,cubic%20foot%20(EIA%202023 (accessed 22 March 2024).
73. United States Environmental Protection Agency (EPA), "eGRID CO_2 total output emission rate (lb/MWh)," Data explorer, https://www.epa.gov/egrid/data-explorer (accessed 22 March 2024).
74. S. Nicholson and G. Heath, "Life cycle emissions factors for electricity generation technologies," NREL Data Catalog, National Renewable Energy Laboratory, Golden, CO (2023).
75. E. Taskesen, "Distfit is a Python library for probability density fitting," 2020, https://erdogant.github.io/distfit (accessed 16 April 2024).

Manish Mosalpuri is a fourth-year PhD student in mechanical engineering at Iowa State University. His research focuses on techno-economic analysis (TEA) and life cycle assessment (LCA) of renewable energy technologies. He has worked on electrochemical conversion of waste nitrates to hydroxylamine, energy conversion and storage using thermophotovoltaics, and solar thermal methane pyrolysis. With experience in modeling and optimization during PhD and masters' research, he aims to advance sustainable energy solutions.

Fatima Toor is an associate professor of electrical and computer engineering and the Lowell G. Battershell Chair in Laser Engineering at the University of Iowa. She also holds a secondary appointment in physics and astronomy. She specializes in semiconductor optoelectronics, with research areas including chemical sensing, biomedical imaging, and energy generation. She is a senior member of Optica and SPIE and has published numerous papers in her field.

Mark Mba-Wright is an associate professor in mechanical engineering at Iowa State University. He specializes in techno-economic and life-cycle analysis of energy systems, focusing on carbon-negative energy technologies. With over 60 publications, his research is sponsored by ARPA-e, NSF, and other federal and private agencies. He chairs the American Institute of Chemical Engineers Sustainable Engineering Forum.